Sterically crowded diphosphinomethane ligands: molecular structures, UV-photoelectron spectroscopy and a convenient general synthesis of $^tBu_2PCH_2P^tBu_2$ and related species†‡

Frank Eisenträger,[a] Alexander Göthlich,[a] Irene Gruber,[a] Helmut Heiss,[a] Christoph A. Kiener,[a] Carl Krüger,[a] J. Ulrich Notheis,[a] Frank Rominger,[a] Gunter Scherhag,[a] Madeleine Schultz,[a] Bernd F. Straub,[a] Martin A. O. Volland[a] and Peter Hofmann*[a]

[a] Organisch-Chemisches Institut der Ruprecht-Karls-Universität Heidelberg, Im Neuenheimer Feld 270, D-69120, Heidelberg, Germany. E-mail: ph@phindigo.oci.uni-heidelberg.de
[b] Max-Planck-Institut für Kohlenforschung, D-45466, Mülheim an der Ruhr, Germany

A series of highly crowded symmetric and unsymmetric diphosphinomethanes $R_2PCH_2PR'_2$, important ligands in transition metal chemistry and catalysis, namely $^tBu_2PCH_2P^tBu_2$ (dtbpm, **1**[1]), $Cy_2PCH_2PCy_2$ (dcpm, **2**), $^tBu_2PCH_2PCy_2$ (ctbpm, **3**), $^tBu_2PCH_2P^iPr_2$ (iptbpm, **4**) and $^tBu_2PCH_2PPh_2$ (ptbpm, **5**), has been prepared in high yields, using a general and convenient route, which is described in detail for **1**. Other than **4**, which is a colourless liquid, these compounds are crystalline solids at room temperature. Their molecular structures have been determined by single crystal X-ray diffraction, along with that of the higher homologue of **1**, $^tBu_2CH_2CH_2^tBu_2$ (dtbpe, **6**). The solid-state structures of the dioxide of **1**, $^tBu_2P(O)CH_2P(O)^tBu_2$ (**7**), and of two phosphonium cations derived from **1**, protonated $[^tBu_2P(H)CH_2P^tBu_2]^+$ (**8⁺**) and the chlorophosphonium ion $[^tBu_2P(Cl)CH_2P^tBu_2]^+$ (**9⁺**), are also described and show a distinct structural influence of the tetracoordinate P centres. The gas phase UV-photoelectron spectra of the diphosphines **1–6** have been measured. Their first two ionisation potentials are found to be nearly degenerate and all are in the low energy range from 7.5 to 7.8 eV. Comparison with related mono- and bidentate phosphines demonstrates that **1–6** are excellent σ-donors towards metals, in accord with their known coordination chemistry. Molecular geometries and electronic structures of the diphosphine systems have been studied by quantum chemical calculations and are compared to experiment. Unlike standard semiempirical methods (AM1, PM3, MNDO), which give rather poor minimum structures and seem inadequate for such sterically crowded systems, *ab initio* calculations (RHF/6-31G**) predict molecular geometries with reasonable accuracy and reflect the observed trends in experimental ionisation potentials.

Introduction

Coordination of bidentate phosphines with a small bite-angle often leads to transition metal complexes that show unusual behaviour.[2] In particular, diphosphinomethane-κ^2P complexes incorporating metal centres into four-membered MPCP-chelate rings have been shown to exhibit unprecedented properties and reactivity patterns. Sterically bulky phosphorous substitution stabilises such four-membered chelate structures in several ways. As a consequence of the so-called geminal dialkyl effect,[3] the use of sterically demanding substituents at the phosphorous atoms of diphosphinomethane ligands engaged in κ^2P bonding allows for a reduction of ring strain, which is inherently present in four-membered MPCP chelate structures and normally favours their ring opening. Moreover, substitution with four bulky alkyl groups hampers the formation of binuclear species with the diphosphinomethane ligand in its otherwise preferred and very common μ-PCP bridging function between two metal centres.[4–8] Sterically demanding alkyl substitution also stabilises ligand-to-metal bonding by increasing the σ-donor strength of diphosphinomethane ligands relative to those bearing smaller alkyl substituents, and protects the metal centre through the steric bulk of the substituents, kinetically hampering side reactions and decomposition.[9]

Using the extremely bulky ligand system $^tBu_2PCH_2P^tBu_2$ [bis(*di-tert-b*utylphosphino) *m*ethane, *dtbpm*, **1**] in such a bidentate mode, novel coordination and reaction chemistry has been studied extensively for various transition metals, oxidation states and *d*-electron counts. We and others have been able to generate highly strained nickel triad 14 valence electron fragments [(dtbpm-κ^2P)M(0)] with a d^{10} electron count (M = Ni, Pd, Pt) as reactive, high energy intermediates *in situ*.[8,10–12] In these intermediates, the P–M–P angle within the MPCP chelate unit deviates by around 100° from the linear equilibrium geometry of non-chelated d^{10}-ML_2 systems, which leads to unusual bond activation chemistry[13–15] and bonding capabilities.[16–20] Employing **1** as a ligand for metals with partially filled *d* valence shells has led to the development of novel types of ruthenium carbene complexes [(dtbpm-κ^2P)(Cl)Ru=CHR]⁺ as highly active olefin metathesis catalysts for ROMP,[21,22] observation of the first reversible C=C bond activation of a ketene using [(dtbpm-κ^2P)Ir]⁺ as a template,[23,24] and characterisation of the first stable three-coordinate alkyl

complex of rhodium, $(\text{dtbpm-}\kappa^2P)\text{Rh}(\text{CH}_2{}^t\text{Bu})$.[25] Cationic complexes $[(\text{dtbpm-}\kappa^2P)\text{M}(\text{R})]^+$ (M = Ni, Pd) and related systems with other bulky diphosphinomethanes have been shown to be efficient catalysts for ethylene/CO and ethylene polymerisation.[26–31] Thus, the use of bulky diphosphinomethanes, and of **1** in particular, has led to many unusual structures and reactions, making these molecules attractive ligands. Parenthetically, we note that chiral variants of bulky diphosphino-alkanes $\text{R}'\text{RP}(\text{CH}_2)_n\text{PRR}'$ (n = 1, 2) have recently been synthesised by Imamoto *et al.*[32] and have been shown to be versatile and attractive ligands for enantioselective metal-catalysed hydrogenation.

Not surprisingly, the utility of these ligands has initiated many efforts to develop synthetic routes for various representatives of this class of compounds. For **1**, the first preparation of a small, spectroscopically identified sample, which was not purified, was reported by Karsch in 1983.[33] The need in our group to easily access reasonable quantities of **1** resulted in the development of a convenient preparative procedure, which was first disclosed in a patent in 1991[34] and which allows the synthesis of **1** on a 50–100 g scale in one run. A slightly modified version of this synthesis was included in a polyolefin patent disclosed by Brookhart *et al.* in 1997.[35] An updated and optimised version of our procedure is described in the Experimental of this paper as a representative case of a general, high yield route to $\text{R}_2\text{PCH}_2\text{PR}'_2$ ligand systems including **1–5** (Fig. 1), which can easily be extended to a variety of other phosphine-containing molecules.

Several compounds in this series have also been prepared by other groups.[33,36–38] These reported synthetic routes, however, are often hampered by low yields of sometimes impure products or are relatively inconvenient. For bis(dicyclohexylphosphino)methane (dcpm, **2**), which is commercially available, an early mention of its preparation and its use as a ligand by Jonas in 1988[39] formed the impetus for our own dtbpm synthesis. Ligand **2** was also independently prepared by Roundhill *et al.*in 1991,[40] and later work of Rothwell described the ''catalytic'' hydrogenation[41] of $\text{Ph}_2\text{PCH}_2\text{PPh}_2$ (dppm) to **2**.[42]

The only general synthesis for $\text{R}_2\text{PCH}_2\text{PR}'_2$ systems available in the literature was reported recently by Werner *et al.*.[38] Among other diphosphinomethanes and some arsino(phosphino)methanes, **2**, dicyclohexylphosphinodi-*tert*-butylphosphinomethane (ctbpm, **3**) and di-*iso*-propylphosphinodi-*tert*-butylphosphinomethane (iptbpm, **4**) are reported using a route *via* stannylated monophosphine precursors. We include **2**, **3** and **4** in the present study because preparation by our route is more general, avoids tin intermediates and yields all compounds except iptbpm (**4**), which is a liquid at room temperature, as white, crystalline solids [not liquids as has been reported for **1**,[33] **3**[38] and diphenylphosphinodi-*tert*-butylphosphinomethane (ptbpm, **5**)[36,37]]. This has allowed their structural investigation by X-ray diffraction, and we report here the solid-state structures of **1**, **2**, **3** and **5**. The structure of **1** is compared to that of its higher homologue
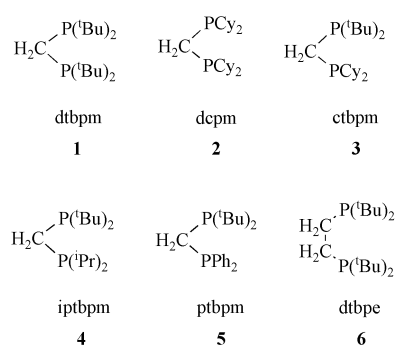
bis(di-*tert*-butyl)phosphinoethane (dtbpe, **6**), another important ligand, and to those of its dioxide ${}^t\text{Bu}_2\text{P}(\text{O})\text{CH}_2\text{P}(\text{O}){}^t\text{Bu}_2$ (**7**) as well as the cations of two phosphonium derivatives of this diphosphine, namely protonated **1**, $[{}^t\text{Bu}_2\text{P}(\text{H})\text{CH}_2\text{P}{}^t\text{Bu}_2]^+$ (**8$^+$**), and the chlorophosphonium salt $[{}^t\text{Bu}_2\text{P}(\text{Cl})\text{CH}_2\text{P}{}^t\text{Bu}_2]^+$ (**9$^+$**).

In phosphorous chemistry, photoelectron spectroscopy (UV-PES) has been used to characterise the valence electronic structure of neutral phosphine ligands.[43–46] It has been shown that the lower the first (lone pair) ionisation energy of phosphine ligands, the better they are as donors in a coordinative bond. Photoelectron spectroscopy is thus one of the few physical measurements that can assess—at least in a qualitative sense—the electronic properties and behaviour of ligands in the absence of metals. The PE spectra of the ligands **1–6** described here are reported and compared with the corresponding values for monodentate and less bulky bidentate phosphines in the literature.

Theoretical studies of the geometries and ionisation potentials of the bidentate phosphine systems **1–6** are also reported. Standard semiempirical methods (AM1, PM3, MNDO[47]) fail and *ab initio* calculations (Gaussian 98, RHF/6-31G**) are employed in order to evaluate the applicability and the predictive value of such calculations for this specific and unusual class of ligand systems. A direct comparison is made between the solid-state structural data and the optimised geometries. The measured ionisation energies are compared with those predicted from the calculated orbital energies, testing the validity of Koopmans' theorem for these systems.

Results and discussion

Synthesis

Our general route to methylene-bridged diphosphines, originally developed for **1**,[34] follows Scheme 1 (full details are provided in the Experimental). Using this route, the related bidentate phosphine ligands **2**, **3**, **4** and **5** (Fig. 1) were also easily prepared by employing the corresponding dialkyl or diaryl chlorophosphines.

Although the use of Grignard reagents to prepare dialkyl-chlorophosphines is long established,[48,49] the yields and purity of the resulting magnesium complexes were not sufficient for efficient synthesis in the quantities required. Therefore, the procedure has been modified by using dioxane after the reaction to precipitate the MgCl$_2$-dioxane complex, which allows ready filtration followed by distillation of the phosphine chloride in high yield. In the subsequent steps, accurate titration of the lithium reagents immediately before use proved key to improving yields.[50] The water for all aqueous solutions must be held at reflux under argon for at least several hours to ensure complete removal of O$_2$, which otherwise leads to contamination by phosphine oxides.

Fig. 1 Bidentate phosphine derivatives used in this study, their acronyms and numbering scheme.
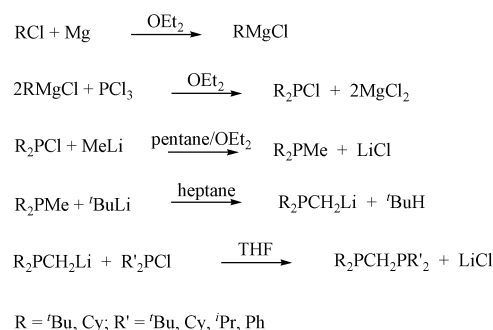
Scheme 1 General synthetic route to methylene-bridged bidentate phosphine ligands.

The key step to the synthesis is the lithiation of the dialkyl-methylphosphine, reported first by Karsch and Schmidbaur.[51] As this reaction proceeds only slowly, even at high temperature, the commercially available pentane solution of *tert*-butyl lithium must be taken to dryness and the solid *^{t}*BuLi redissolved in heptane before addition of the dialkylmethylphosphine as a heptane solution and heating to reflux. The formed lithium methanide derivative is pyrophoric, and to avoid possible contact with air, a short, wide neck containing a frit and ending in a ground glass joint was attached beforehand by blown glass to a round-bottomed flask, which is used for this reaction. The joint is capped during the reaction, and after the 18 h at reflux are complete, the cap is replaced by another Schlenk flask. The insoluble product is then separated from the liquor by tilting the flask so that the solution flows through the frit.[52] The final step yields the product diphosphines, which are very oxygen-sensitive but water stable and not thermally sensitive. Other than **1**, the diphosphines can be crystallised from pentane; **1** itself can be most cleanly obtained from methanol.

Solid-state structures

All of the ligands except the colourless liquid **4** are white, crystalline solids at ambient temperature, and the crystal structures of the solid diphosphines have been determined. The molecular structure of **2**, prepared according to Scheme 1, was mentioned in a footnote of a paper by one of the present authors some time ago.[10] Details of this structure are now provided for comparison with the other diphosphines reported. In the case of **1**, severe disorder in the crystal leads to inaccuracy in the structural data; the structural problem is described in the Experimental.

Fig. 2 shows, as a representative example, an ORTEP diagram of **3**. ORTEP diagrams for all crystallographically characterised molecules are provided in the electronic supplementary information (ESI). Important bond distances and angles for all of the structures are contained in Table 1, while relevant data collection and structure solution parameters are provided in Table 2. In each molecule, the lone pairs of the two phosphorous atoms point away from each other, with dihedral angles of between 56° and 100°. This dihedral angle of the diphosphines was determined by situating dummy atoms (X and X′) at the calculated centroids of the three carbon atoms bound to each phosphorous atom (P and P′), and then measuring the torsion angle X–P–P′–X′. Rotation about the P–C bonds is expected to be facile in solution, and the variation in dihedral angle in the observed structures is unlikely to be chemically significant. The angles about the bridging carbon atom range from 110° to 120°; these angles in **1**, **2** and **3** of around 120° are significantly higher than the ideal tetrahedral angle. This distortion is presumably related to the steric bulk of the adjacent groups and is reproduced in calculations (see below).
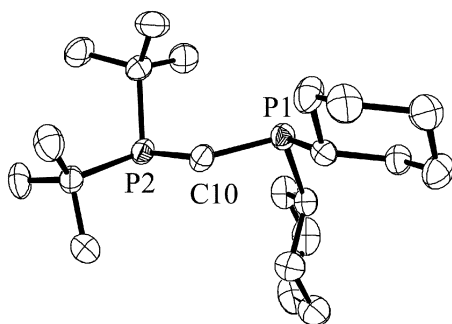

Fig. 2 ORTEP diagram (50% probability ellipsoids) of **3**. Hydrogen atoms have been omitted for clarity.

As chelating ligands, the diphosphines have to deviate drastically from these solid-state geometries. The P–C–P bond angle must reduce by around 20° to reach the values of around 95–100° typical in structures containing a methylene-bridged diphosphine ligand, and the dihedral torsion is removed.[9,16,17,53] The existence of a large body of solid-state structure determinations in which **1** acts as chelating ligand shows that the distortions required for κ²-ligation to a transition metal centre are easily accomplished.[54]

The melting point of **2** (95–97 °C) is much higher than that of the other diphosphines studied in this work. The calculated density of the crystal is 10% higher than those of the other ligands at 1.113 g cm⁻³ (Table 2), although not as high as those of the oxidised phosphines, which indicates that this molecule packs more efficiently than **1**, **3** and **5**. For comparison, the melting point of dppm is 120–122 °C,[55,56] and the calculated density in the crystal is 1.254 g cm⁻³.[57] A possible structural reason for the high density of **2** can be seen in the packing diagram shown in Fig. 3. The cyclohexyl groups are arranged in a dense manner within the crystal, interleaving with cyclohexyl groups from adjacent molecules. The flat phenyl groups of dppm presumably allow still denser packing in that molecule, while the bulkier *tert*-butyl and *iso*-propyl substituents in **1**, **3**, **4** and **5** prevent it. Fig. 4 shows a packing diagram of **5** for comparison; it can be seen that the individual molecules do not interleave, resulting in a lower density.

The sum of the three C–P–C angles of a phosphine gives an indication of the hybridisation of the phosphorous atom and is related, although not directly, to the Tolman cone angle. The pyramidalisation of the phosphines in the structures presented here can be compared with that in the crystal structures of PMe₃ and P(*^{t}*Bu)₃, in which the sums of the angles about P are 298°[58] and 322°,[59] respectively. The sums of angles about the phosphorous atoms bearing *tert*-butyl groups in the bidentate ligands **1**, **3** and **5** are close to 314° in each case. This reflects the steric bulk of two *tert*-butyl groups; the phosphorous geometry is not as flattened as in P(*^{t}*Bu)₃ but less pyramidalised than phosphorous atoms with three smaller substituents. When **1** acts as a chelating ligand, the phosphorous atoms are flatter; the sums of C–P–C angles about the phosphorous atoms are above 320°,[16,17] due to the smaller repulsive effect of electrons in a dative P–M bond relative to a lone pair. The phosphorous atoms in the bidentate phosphines **2**, **3** and **5** bearing cyclohexyl or phenyl groups are somewhat more pyramidalised, with sums of angles of around 304°.

The ethylene-bridged analogue of **1**, dtbpe (**6**), has been used to support interesting chemistry on nickel,[60–66] palladium,[67] platinum[68] and ruthenium.[69–71] In order to compare this ligand with **1**, its structure was also determined crystallographically and an ORTEP diagram is shown in Fig. 5. The centre of the ethylene bridge lies on a special position, resulting in a crystallographically imposed 180° dihedral angle between the lone pairs on phosphorous. The bond distances and angles as well as the pyramidalisation of the phosphorous atoms are similar to those found in **1**. As a chelating ligand, **6** binds with P–M–P angles of around 85–90°, which is easily achieved through rotation around P–C bonds and bending the flexible ethylene backbone.

Oxidation of **1** with hydrogen peroxide led to isolation of the dioxide *^{t}*Bu₂P(O)CH₂P(O)*^{t}*Bu₂ (**7**). This compound was also structurally characterised and an ORTEP stereoview diagram is shown in Fig. 6, while selected bond distances and angles can be found in Table 1 and data collection and structure solution parameters are in Table 2. In comparison to **1**, the geometry of the molecule changes somewhat upon oxidation; the P–C–P angle opens further to 128° and 125° in the two unique molecules, presumably related to the more bulky P(O)(*^{t}*Bu)₂ groups on the bridging carbon atom relative to the P(*^{t}*Bu)₂ groups in the parent ligand, and electrostatic repulsion

Table 1 Selected bond distances (Å) and angles (°) in the molecular structures of **1**–**3** and **5**–**9⁺**

	1	**2**	**3**	**5**	**6**	**7**[a]	**8⁺**	**9⁺**
P–C (bridge)[b]	1.834(9)	1.859(2)	1.855(3)	1.861(2)	1.860(1)	1.837(2), 1.833(2)	1.879(3)	1.906(7)
P–C (bridge)	1.832(9)	1.859(2)	1.863(3)	1.852(3)	Special position	1.833(2), 1.831(2)	1.806(3)	1.803(7)
P–C (bridge)–P	118.4(7)	120.5(1)	120.3(2)	109.7(2)	P–C–C 112.7(1)	128.1(1), 124.8(1)	118.6(1)	118.8(4)
Dihedral angle of lone pairs[c]	95	99	91	56	180	94, 77	65	46
P–X						mean P–O	P–H	P–Cl
						1.48	1.34(2)	1.918(4)
Sum of C–P–C angles[d]	310	303	312	314	315	322, 322	313	312
	314	304	303	304		322, 322	339	338

[a] Data for two unique molecules in the unit cell presented as molecule 1, molecule 2. [b] For the asymmetrical molecules, the first P–C distance involves the P atom bearing *tert*-butyl groups (**3**, **5**) or the P(III) atom (**8⁺**, **9⁺**). [c] The dihedral angle is the torsion angle between a dummy atom located at the calculated centroid of the three carbon atoms bound to P1, P1, P2 and a dummy atom located at the calculated centroid of the three carbon atoms bound to P2. For consistency, for **7**, **8⁺** and **9⁺** the same procedure was used although a lone pair is not always present. [d] For the asymmetrical molecules, the first value listed corresponds to the phosphorous atom bearing *tert*-butyl groups (**3**, **5**) or the P(III) phosphorous atom (**8⁺**, **9⁺**).

between the two oxygen atoms. The P–C (bridge) distances are, however, unchanged from those of **1**. The dihedral angles between the oxygen atoms in the two unique molecules are different from each other: 94° and 77°. This difference is most likely due to packing effects, as the sums of the C–P–C angles in **7** are larger than in **1** but similar in both molecules of the asymmetric unit at 322°. The decrease in pyramidalisation of the phosphorous centres upon oxidation is a consequence of the smaller repulsive effect of the electrons in the P–O bond relative to the repulsive effect of the electrons in the lone pairs in **1**; the corresponding sum of angles in (O)P(ᵗBu)₃ is 339°.[72]

In the context of hydroformylation studies using ligand **1**, protonated **1** was isolated as an unintended side product from a reaction mixture as the triflate [ᵗBu₂P(H)CH₂PᵗBu₂]⁺-[CF₃SO₃]⁻. X-Ray quality crystals of the colourless salt were obtained upon crystallisation from diglyme and a molecular structure determination was performed. As the structural details of the cation of this compound (**8⁺**) seemed important in comparison to **1**, and as a complete spectroscopic characterisation was also desirable, the [BArF]⁻ {BArF = B[3,5-(CF₃)₂C₆H₃]₄} salt of **8⁺** was prepared independently by protonating **1** in diethyl ether with [H(OEt₂)₂]BArF and precipitating the salt with hexane. Good quality crystals were obtained by crystallisation of [**8⁺**][BarF]⁻ from a 1:1 diethyl

ether–hexane mixture at −20 °C. Bond distances and angles are listed in Table 1 and data collection and structure solution parameters are given in Table 2.

Most strikingly, the triply coordinated phosphorous atom of **8⁺** has a much longer P–C distance to the bridging carbon atom (1.88 Å) than that with a proton (1.81 Å). The corresponding value in **1** is 1.83 Å. This is most likely due to the electron-withdrawing effect of the P(v) making a shorter bond to the bridging carbon atom, which leads to a weaker, longer bond to the P(III). In agreement with Bent's rules,[73,74] the central carbon concentrates more *p*-character towards the more electronegative phosphonium group. The P–C–P angle is the same as that in the parent structure, and the torsion angle is smaller than in **1**. The sum of C–P–C angles about the phosphorous bearing the proton is very high (337°), with distinctly less pyramidalisation of the phosphonium PC₃ frame than at the P centres in **1** or **7**, again due to the smaller repulsive effect of electrons in a P–H bond compared with a lone pair. The sum of angles about the P(III) centre is 312°, typical for the CH₂–PᵗBu₂ fragment as in neutral **1** and **6**.

A second dtbpm derivative with one phosphonium group was obtained accidentally when iron derivatives of dtbpm were synthesised. In a reaction of (CO)₄FeCl₂ with **1**, the complex (dtbpm-κ²P)Fe(CO)₃ was isolated in low yield[75] and a second,

Table 2 Selected crystal data and structure solution parameters for **1**–**3**, **5**–**7**, [**8⁺**][B{3,5-(CF₃)₂C₆H₃}₄]⁻ and [**9⁺**][Fe₂Cl₆]₁/₂⁻·CH₂Cl₂

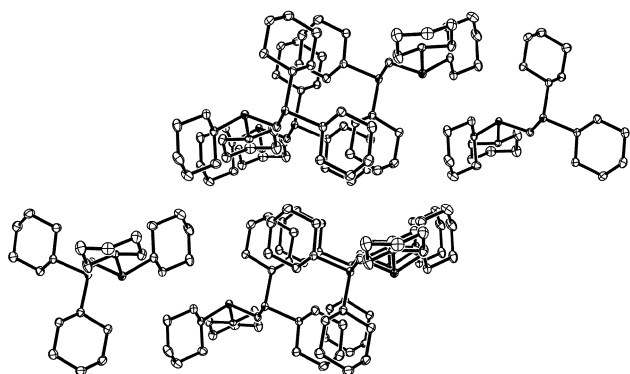|	**1**	**2**	**3**	**5**	**6**	**7**	**8⁺** [B{3,5-(CF₃)₂C₆H₃}₄]⁻	**9⁺** [Fe₂Cl₆]₁/₂⁻·CH₂Cl₂
Formula	C₁₇H₃₈P₂	C₂₅H₄₆P₂	C₂₁H₄₂P₂	C₂₁H₃₀P₂	C₁₈H₄₀P₂	C₁₇H₃₈O₂P₂	C₄₉H₅₁BF₂₄P₂	C₁₈H₄₀Cl₆FeP₂
FW	304.41	408.56	356.49	344.39	318.44	336.41	1168.65	586.99
Crystal system	Orthorhombic	Triclinic	Monoclinic	Monoclinic	Monoclinic	Monoclinic	Monoclinic	Monoclinic
Space group	Pna2₁(#33)	P1̄ (#2)	P2₁/n (#14)	P2₁/c (#14)	P2₁/n (#14)	P2₁/c (#14)	P2₁/n (#14)	P2₁/c (#14)
a/Å	9.3565(1)	9.718(2)	11.1753(5)	6.2975(2)	8.5001(1)	9.5711(2)	16.7907(1)	18.2861(3)
b/Å	17.3925(2)	10.423(2)	9.8062(4)	33.5911(4)	10.1304(2)	25.0934(4)	19.1459(2)	9.9887(2)
c/Å	12.5085(2)	12.775(1)	20.3041(8)	10.2346(2)	12.9111(2)	17.6357(1)	18.2699(2)	17.3272(3)
α/°	90	98.21(1)	90	90	90	90	90	90
β/°	90	96.84(1)	94.633(1)	105.314(1)	106.176(1)	105.061(1)	113.552(1)	113.857(1)
γ/°	90	105.23(1)	90	90	90	90	90	90
U/Å³	2035.54(5)	1219.0(4)	2217.8(2)	2088.15(8)	1067.75(3)	4090.1(1)	5384.02(9)	2894.47(9)
Z	4	2	4	4	2	8	4	4
T/K	233	100	200	200	200	200	200	200
μ(Mo-Kα)calc/mm⁻¹	0.204	0.186	0.196	0.207	0.197	0.216	0.20	1.190
Total reflection	16 625	31 999	18 216	15 312	10 678	30 348	47 177	28 351
Unique reflections	3534	5611	3913	3599	2444	7114	9828	6617
R_{int}	0.0310	0.0868	0.1198	0.0538	0.0331	0.0357	0.0671	0.1251
Obs. reflections [$F_o^2 > 2\sigma(F_o^2)$]	2874	4742	2341	2435	1954	5422	5980	3776
R_1 (obs. data)	0.0405	0.045	0.053	0.046	0.034	0.041	0.047	0.102
wR_2 (obs. data)	0.1103	0.129	0.095	0.088	0.086	0.098	0.098	0.231

Fig. 3 Packing diagram of **2** (50% thermal ellipsoids). Hydrogen atoms have been omitted for clarity.

less soluble product was identified by X-ray crystallography to be [^{t}Bu$_2$P(Cl)CH$_2$P^{t}Bu$_2$]$^+$[Fe$_2$Cl$_6$]$_{1/2}^-$·CH$_2$Cl$_2$. In the cation of this salt, **9$^+$**, the chloro analogue of **8$^+$**, the phosphorous atom bound to chlorine has also been oxidised to P(v). The structure of this cation provides another comparison with **1**, **7** and **8$^+$** and thus has been included here. Important bond distances and angles are listed in Table 1 and data collection and structure solution parameters are given in Table 2. The structural features of cation **9$^+$** are very similar to those of cation **8$^+$**; in particular, the distance from the triply coordinated phosphorous atom to the bridging carbon atom C10 is again very long, even longer than in **8$^+$**, in line with expectations from Bent's rules (1.91 Å as compared to 1.83 Å in the parent **1**), while that from the P(v) centre is short (1.80 Å). The P–C–P angle of **9$^+$** as in **8$^+$** is not different from that of **1**, but the phosphorous atom bearing the chloride is also in the centre of a much flatter alkyl environment (sum of C–P–C angles 338°), as described for **8$^+$**. The sum of C–P–C angles about the other phosphorous atom is also typical for the CH$_2$–P^{t}Bu$_2$ fragment (312°).

Comparing all seven solid-state molecular structures with a P–C–P skeleton, the basic features of these bulky diphosphino-methane ligands and the related oxidised phosphines are a P–C–P angle that is larger than for an idealised sp^3 geometry at carbon (except **5**), a twisted core that points the lone pairs (or substituents) on the phosphorous atoms away from each other, and relatively flat phosphorous geometries. The last feature can be readily explained by the steric bulk of the substituents on the phosphorous. In the cases where a fourth substituent is bound to an oxidised P(v) atom, the three alkyl substituents form an even less pyramidal (although not planar) coordination environment, with the oxygen, hydrogen or
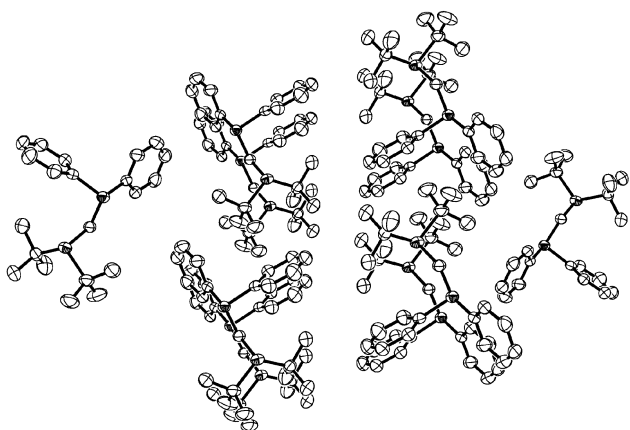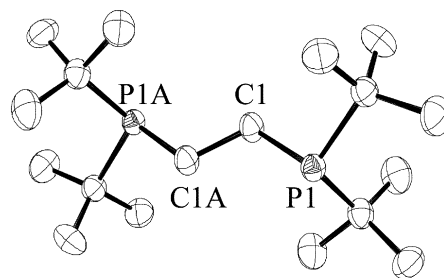

Fig. 5 ORTEP diagram (50% probability ellipsoids) of **6**. Hydrogen atoms have been omitted for clarity.

chlorine atom above this plane, due to the smaller repulsive effect of a bonding electron pair relative to a lone pair on phosphorous.

Electronic structure and photoelectron spectroscopy

As described above, some aspects of the solid-state structures are of chemical significance, as they relate to the hybridisation at phosphorous, to the character of the lone pairs, to the bite-angle and thus to the coordination and ligand properties. In an attempt to quantify and understand the significance of the structures in the crystalline state, and to relate them to gas phase structures and gas phase photoelectron spectroscopy, quantum chemical calculations have been carried out.

Semiempirical calculations at the AM1, PM3 and MNDO level[47] on the diphosphine systems **1**–**9$^+$** revealed that the P–C–P angles at the methylene bridges are generally badly over-estimated (by 10–20°) in the optimised geometries at this level of theory. For the compounds with P(v) centres, this angle is also far too high in the calculated structures (*ca.* 140°). Furthermore, the sum of the angles about the P(III) atoms is overestimated by about 10° in every case, making the pyramidalisation at phosphorous distinctly smaller than what is observed. The large difference in P–C bond lengths to the bridging carbon atoms found in the crystal structures of the phosphonium cations **8$^+$** and **9$^+$** is reproduced in the calculations, but the calculated bond length to the P(III) atom is too short. The pronounced deviations from experimental geometries probably have to do with the fact that highly crowded phosphines—unlike sterically less congested, "normal" ones, where semiempirical models perform better—fall outside the range of systems utilised in parametrising these methods. Therefore, geometric predictions are not valid and *ab initio* calculations at an appropriately high level of theory (RHF/6-31G**) were performed for all systems, **1**–**9$^+$**.

Fig. 4 Packing diagram of **5** (50% thermal ellipsoids). Hydrogen atoms have been omitted for clarity.
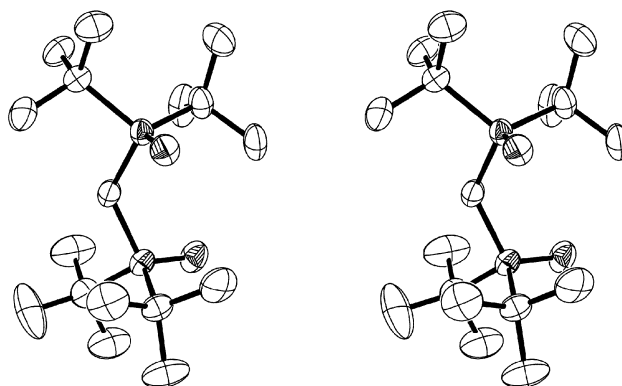

Fig. 6 Stereoview ORTEP diagram (50% probability ellipsoids) of dioxide **7**. Only one of the two independent molecules in the asymmetric unit is shown. Hydrogen atoms have been omitted for clarity.

Table 3 Selected bond distances (Å) and angles (°) of optimised structures (RHF/6-31G**) of the bidentate phosphines 1–9$^+$

	1	2	3	4	5	6	7	8$^+$	9$^+$
P–C (bridge)^a	1.876	1.869	1.878	1.875	1.861	1.876	1.850	1.899	1.908
P–C (bridge)	1.877	1.869	1.878	1.860	1.852	1.876	1.850	1.827	1.828
P–C (bridge)–P	120.2	118.9	118.4	117.0	109.7	P–C–C 112.7	126.0	122.0	125.3
Dihedral angle of lone pairs^b	86	92	92	83	56	178	91	84	88
P–X							P–O 1.48	P–H 1.39	P–Cl 2.01
Sum of angles about P^c	314	306	314	314	314	316	323	314	314
			317	311	304			338	338

^{a} For the asymmetrical molecules, the first P–C distance involves the phosphorous atom bearing *tert*-butyl groups (**3**, **4** and **5**) or the P(III) phosphorous atom (**8**$^+$, **9**$^+$). ^{b} The dihedral angle is the torsion angle between a dummy atom located at the calculated centroid of the three carbon atoms bound to P1, P1, P2 and a dummy atom located at the calculated centroid of the three carbon atoms bound to P2. For consistency, for **7**, **8**$^+$ and **9**$^+$ the same procedure was used although a lone pair is not always present. For **7**, the mean P–O bond distance is given, for **8**$^+$ the P–H distance and for **9**$^+$, the P–Cl distance. ^{c} For the asymmetrical molecules, the first value listed corresponds to the P atom bearing *tert*-butyl groups (**3**, **4** and **5**) or the P(III) atom (**8**$^+$, **9**$^+$).

Selected distances and angles of the RHF/6-31G** optimised geometries of **1–9**$^+$ are included in Table 3, and a diagram of the minimum energy geometry calculated for ctbpm (**3**) is shown in Fig. 7, which can be compared with the crystallographically determined structure in Fig. 2. It can be seen that the calculated geometries generally resemble the solid-state structures. Although the absolute values of the distances and angles calculated for the gas phase minimum structures are not (and cannot be expected to be) precisely identical to the values found in the solid state, the deviations are small or insignificant, and the trends in bond lengths, torsion angles and P–C–P angles within the six crystallographically characterised neutral molecules and the two cations are reproduced remarkably well by the calculations. The P–C (bridge) distances are slightly overestimated for most of the ligands, but the calculated P–C–P angles are close to those observed. Even the predicted dihedral angles of the lone pairs are similar to the observed values, except in the two cations, for which the predicted dihedral angles are higher than those found in the molecular structures. In addition, for the two cations, the P–X distance is calculated to be somewhat higher than that observed, while in the dioxide (**7**) the prediction is accurate. The pyramidalisation about the P centres is predicted extremely well for both the P(III) and P(V) atoms of all 8 complexes studied crystallographically.

Calculations at the RHF/6-31G** level therefore provide a reasonable method to assess the structural characteristics of this type of ligand in the gas phase and even give an approximate picture of the conformations adopted in the solid state by these rather unpolar molecules.

In order to quantify the σ-donor character of these electron-rich diphosphines, especially in comparison to other monodentate or chelating phosphine ligands, the UV-photoelectron spectra of **1–6** were measured. The ionisation potentials, taken as the maximum of the first broad ionisation band in the spectrum of each compound (which actually represents the two lowest energy ionisation events) are given in Table 4. Note that in the PE study of Puddephatt *et al.* involving the uncongested diphosphines dmpm and dmpe, a single "ionisation energy of the phosphorus lone pair" was described; the PE spectra also showed only one unresolved first ionisation peak, which was deconvoluted to an ideal Lorentzian–Gaussian shape but must contain the two ionisation events from both P lone pairs at slightly different energies.[45] The spectra of **1–6** are all very similar, with the first two ionisation potentials around 7.6 eV; a representative spectrum of **1** is shown in Fig. 8. The second ionisation potential is not resolved experimentally (except in the case of **5**, where two peaks at 7.5 and 7.6 eV can be assigned), as it lies within 0.2 eV of the first ionisation potential in each case. All PE spectra (compounds **1–6**) are provided in the ESI.

The first two ionisations of the diphosphines correspond to ionisation of the phosphorous lone pair electrons. Assuming the validity of Koopmans' theorem ($-\varepsilon_j = \mathrm{IP}_j$), which should be allowed in these organic systems, the first two ionisations correspond to the two canonical, non-degenerate, symmetry-adapted highest occupied molecular orbitals, which are the linear combinations of the two P lone pairs, delocalised to some extent into the P–C and C–C bonds. Comparison with the values reported for monodentate PMe$_3$ (8.59 eV)[46] and P(^{t}Bu)$_3$ (7.70 eV)[43] as well as the less bulky bidentate ligands bis(dimethylphosphino)methane (dmpm) (8.43[46] or 8.51 eV[45]) and bis(dimethylphosphino)ethane (dmpe) (8.45[46] or 8.47 eV[45]) shows that the diphosphines reported here are much more readily ionised than their methyl-substituted analogues,
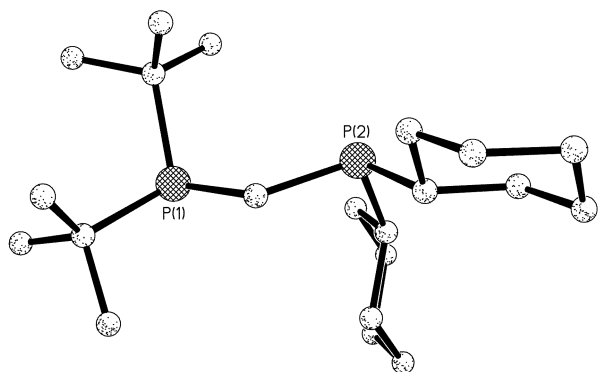

Fig. 7 Calculated minimum geometry for **3** (RHF/6-31G**). Hydrogen atoms have been omitted for clarity.

Table 4 Measured ionisation potentials (eV) and calculated orbital energies (HOMO, HOMO–1) from the optimised geometries of diphosphines **1–6** (RHF/6-31G**)

	1	2	3	4	5	6
Measured^a	7.8	7.7	7.6	7.7	7.5, 7.6	7.8
HOMO	8.24	8.39	8.34	8.30	7.90	8.19
HOMO–1	8.39	8.46	8.45	8.45	8.22	8.46
Δ(HOMO–1) − (HOMO)	0.15	0.07	0.11	0.15	0.32	0.27

^{a} The value given corresponds to the centre of the first broad ionisation band in the PE spectrum, which comprises the first two ionisation events. For **5**, the first two ionisation potentials are resolved (see Fig. 10).
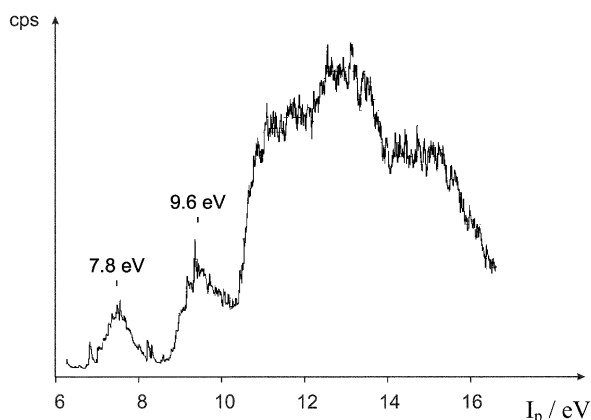
Fig. 8 UV-photoelectron spectrum of **1**.

Fig. 10 UV-photoelectron spectrum of **5**.

and resemble P(^{t}Bu)$_3$ in their σ-donor capabilities. The reported values for phenyl-substituted phosphines such as PPh$_3$ (7.88[76] or 7.80 eV[77]), dppm (7.79 eV) and bis(diphenyl-phosphino)ethane (dppe) (7.86 eV)[45] are closer to those observed for the ligands here, for reasons discussed below.

Ab initio RHF/6-31G** calculations predict energies of the HOMO and HOMO-1, corresponding to the first two ionisation energies of the diphosphines **1**–**6**. Values have been obtained using completely optimised geometries (NIMAG = 0) and the results are included in Table 4. Fig. 9 shows plots of the calculated HOMO and HOMO-1 for **1**. As expected, the two frontier MOs correspond to the in- and out-of-phase combinations of the lone pairs. The data in Table 4 shows that the calculations consistently overestimate the ionisation potentials by, on average, 0.5 eV. However, the energy split between calculated HOMO and HOMO-1 is always small, which agrees well with the experimental observations.

Apart from ionisations at 7.5 and 7.6 eV, the photoelectron spectrum of **5** (Fig. 10) exhibits bands at 8.8–10 eV, which are not observed in the other spectra. They are attributed to the ionisation from the phenyl rings in that compound. This interpretation, which is in line with interpretations of the PE spectra of other phenyl-substituted phosphines,[45,76–78] is verified by the RHF/6-31G** HOMO-2 and HOMO-3 wave functions shown in Fig. 11 for the optimised geometry of **5**. Clearly, these two orbitals do involve electron density mostly in the aromatic rings, so the assignment seems to be reasonable. The HOMO and HOMO-1 of **5** have similar appearances to those orbitals displayed for **1** and again represent ionisation from the two phosphorous lone pairs. It is worth noting that phenyl-substituted phosphines like PPh$_3$ (7.80 eV)[77] and dppm (7.79 eV)[45] have rather low ionisation potentials, in the same range as those found for **1**–**6**, but in this case they are caused by conjugative interactions between the P centre and the aryl rings, that is by a particular stabilisation of the radical cations formed upon ionisation. In these fully phenylated systems, the difference between one-electron (MO energies) and collective properties (ionisation) becomes particularly relevant and thus
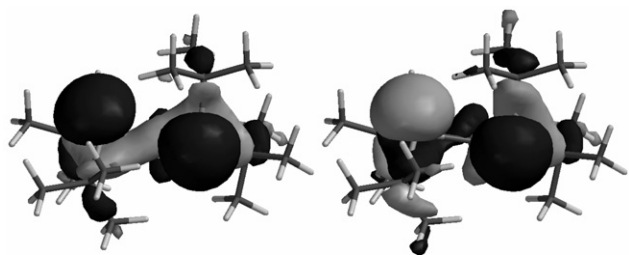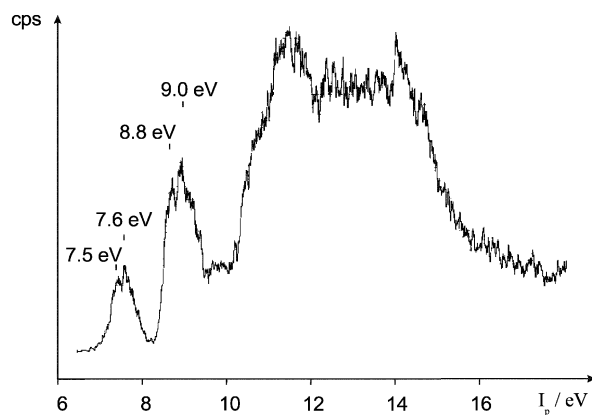
Koopmans' theorem breaks down.[78] The broad band observed above 10 eV in all of the photoelectron spectra reported here is due to ionisations from P–C bond orbitals and from the alkyl substituents on the phosphorous atoms.

A referee has pointed out that the consistent deviation of observed ionisation potentials for **1**–**6** from those values derived *via* Koopmans' theorem from HOMO and HOMO-1 energies might be a consequence of a stabilisation of the radical cations through geometric relaxation and concomitant formation of cyclic structures with a weak, 2-centre/3-electron P–P interaction. We refrain from such an interpretation because, unlike in the condensed phase, electron removal in a PE experiment is a fast process that does not lead to a relaxation of the molecular structure. We therefore see the discrepancy of (on average) 0.5 eV between measured ionisation potentials and calculated orbital energies as resulting from electronic reorganisation, caused by removing electrons from strongly localised (P lone pair) orbitals, as is well known for *d*-orbitals in transition metal compounds, where such Koopmans' defects often forbid the correlation of ground state orbital energies with ionisation energies. The large organic groups attached to the P centres in **1**–**6** are potent electron reservoirs and particularly suited for efficient electron density relaxation towards the ionised centres. The assumption of an incipient P–P interaction upon ionisation and of stabilised cyclic radical cations is also inconsistent with diphosphinoethane (**6**) showing exactly the same behaviour as **1**–**5**. A change from the ground state geometry of **6** (Fig. 5, Tables 1, 3) to a four-membered ring structure with P–P 2-centre/3-electron bonding during the PE ionisation event seems highly improbable. Moreover, in a cyclic radical cation of this type, through-bond coupling[79] would lead to a SOMO of n_+ character and to no net P–P attraction upon ionisation. For diphosphinomethanes with a methylene unit between the two P atoms this is different; calculations with complete geometry optimisation for the radical cation of dmpm at the UB3LYP/6-31G** level of theory lead to two separate minima (NIMAG = 0), one with a closed structure
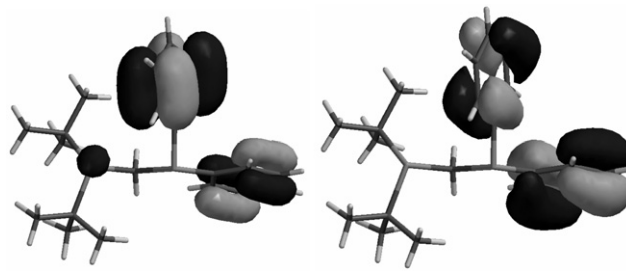

Fig. 9 Plots of the calculated HOMO (left) and HOMO–1 for **1** (RHF/6-31G**).

Fig. 11 Contour plots of the calculated HOMO–2 and HOMO–3 for **5** (RHF/6-31G**).

(P–C–P = 89.6°, P–P = 2.62 Å) and one with an open geometry (P–C–P = 113.3°, P–P = 3.12 Å). The latter is only 1.36 kcal mol^{-1} more stable than the former (for details see ESI).

The difference in energies between the geometry optimised ground state structures of **1**–**6** and their radical cation ground states computed for the same geometry and at a sufficiently high level of theory would give the first ionisation potentials for these systems without having to resort to Koopmans' theorem. We did not perform such calculations for these large molecules, because despite the systematic small deviations in absolute values, the ground state *ab initio* calculations at the RHF/6-31G** level allow a consistent interpretation of all PE spectra.

Conclusions

A convenient, flexible and clean synthetic route to highly substituted, methylene-bridged diphosphine ligands has been established. The crystal structures of compounds prepared by this route show some characteristic common features. The P–C–P angles lie in the range 110–120°, which is distinctly larger than the ideal tetrahedral angle about carbon; this distortion is related to the steric bulk on the two adjacent phosphorous atoms. The phosphorous atoms have relatively flat coordination substituent environments compared with methyl-substituted phosphines, which lead to greater *p* character in their lone pairs. This can be observed in the photoelectron spectra, which show these bulky diphosphinomethanes to have very low, nearly degenerate first and second ionisation potentials for the two P lone pairs, making them different from smaller, bidentate phosphines such as dmpm. The ease of oxidation predicted by the photoelectron spectra is illustrated by the air sensitivity of the ligands and the preparation of the dioxide of **1**, **7**.

Ab initio theory at the RHF/6-31G** level is a fast and quite reliable tool to predict the molecular and electronic structures of these phosphines, yielding optimised geometries that closely reflect the solid-state structures. The trends of structural changes induced by oxidation of both P atoms [dtbpm (**1**) *vs.* (**7**)] or by transforming one of the P centres into a phosphonium unit, as in **8**$^+$ and **9**$^+$, are reflected correctly. Assuming the validity of Koopmans' theorem, the ionisation potentials are predicted with an error of (on average) 0.5 eV for all ligands in this series.

The photoelectron spectra and calculations illustrate the special nature of diphosphinomethane ligands with bulky substituents. These compounds are much better donors (for example towards Lewis acidic metal centres) than diphosphine ligands with smaller substituents, due to the high energy and high *p* character of their P lone pairs, and they form strongly stabilised structures when they bind to a metal to form a four-membered chelate ring system. This provides a physical and theoretical basis for understanding the resulting unique organometallic and metal complex chemistry displayed by these ligands.

Experimental

General

All reactions and product manipulations were carried out under dry argon using standard Schlenk and dry box techniques unless otherwise indicated. Dry, oxygen-free solvents were employed throughout except where noted. The elemental analyses were performed by the Mikroanalytisches Laboratorium der Chemischen Institute der Universität Heidelberg. Photoelectron spectra were measured at room temperature on a PS18 spectrometer from Perkin–Elmer and calibrated

with Xe and Ar. The resolution of the $^2P_{3/2}$ line of Ar was 20 meV.

The chlorophosphines $^tBu_2PCl$, Cy_2PCl and $^iPr_2PCl$ were prepared from freshly distilled PCl_3 and the corresponding Grignard reagent in diethyl ether.[43,48,49] A modification of the published procedure was used and the precise conditions used are described below for $^tBu_2PCl$. ^tBuCl was dried over Na/Pb and distilled freshly before use. Methyl lithium and *tert*-butyl lithium were purchased in solution from Fluka and their exact concentrations were determined by titration before each use. Ph_2PCl was purchased from Aldrich and used without further purification. Ethylene-bridged dtbpe (**6**) was prepared according to the method of Pörschke *et al.*.[80] $Pd(OAc)_2$ was purchased from Aldrich. $(CO)_4FeCl_2$ was prepared according to the literature.[81]

Syntheses

dtbpm (1). *Step 1: ^tBuMgCl.* Mg turnings (97.4 g, 4.0 mol) were weighed into a 2 L three-necked flask equipped with a reflux condenser, a graduated, pressure-equalising dropping addition funnel and a large magnetic stirrer bar. To activate the Mg turnings, they were heated under vacuum and then stirred overnight at room temperature under Ar. Diethyl ether (200 mL) was added. ^tBuCl (250 mL, 3.7 mol) was transferred to the addition funnel *via* cannula and as much added to the reaction flask (*ca.* 20 mL) as required for initiation of the Grignard reaction. After the reaction began, the ^tBuCl in the addition funnel was diluted with 200 mL diethyl ether. This solution was added at a rate that caused light reflux of the solvent (*ca.* 90 min). The reaction mixture was then heated to reflux for 1 h. After cooling, the grey-black solution was filtered through a D_3 frit with a Celite pad into a graduated Schlenk flask. The residual solid was washed with diethyl ether (2×100 mL) and the washings were filtered into the flask. Titration was performed by the Gilman method.[50] Yield: 600 mL of a 3.19 M solution (1.91 mol) (note that Step 2 functions well on a maximum scale of 2.0 mol)

Step 2: $^tBu_2PCl$. Diethyl ether (1.6 L) was transferred to a 4 L three-necked flask equipped with a gas inlet, overhead stirrer and a 1 L graduated addition funnel. PCl_3 (70 mL, 110 g, 0.80 mol) was added. ^tBuMgCl (600 mL of a 3.19 M solution in diethyl ether, 1.91 mol) was cannulated into the addition funnel and diluted with a further 300 mL diethyl ether. This solution was then added to the PCl_3 solution at a rate of 100 mL h^{-1} at -33–-41 °C (dry ice/ethanol bath). After addition of 450 mL, the solution was gradually allowed to warm to room temperature as addition continued at the same rate. The resulting pale viscous suspension was stirred overnight, then the addition funnel was exchanged for a condenser and the mixture was heated to reflux for 30 min. Dioxane (300 mL) was cannulated into the solution through the condenser and the mixture was heated to reflux again for an hour. The suspension became noticeably less thick. This dioxane addition method facilitates the removal of $MgCl_2$ as its less soluble dioxane complex. After cooling to room temperature the mixture was filtered through a frit to separate the ethereal solution from the $MgCl_2$-dioxane complex. The precipitate was washed with diethyl ether (2×250 mL). The diethyl ether was then distilled off at atmospheric pressure and the residue was fractionally distilled under vacuum. The product was collected at 64 °C/12 mbar. Yield: 87.4 g of a colourless liquid (484 mmol, 60% based on PCl_3). ^{1}H NMR (300 MHz, $CDCl_3$, 298 K): δ 1.18 (d, $^3J_{PH} = 12$ Hz). ^{31}P{^{1}H} NMR (121.5 MHz, $CDCl_3$, 298 K): δ 146.2 (s).

Step 3: $(^tBu)_2PMe$. Di(*tert*-butyl)chlorophosphine (76.1 g, 0.421 mmol) was measured into a 1 L flask equipped with a graduated dropping addition funnel and containing a magnetic stirrer bar. The colourless liquid was dissolved in pentane (285 mL) and cooled to -78 °C. Methyl lithium (300 mL of

a 1.6 M solution in diethyl ether, 0.48 mol) was added over 2.5 h and washed through with a further 100 mL diethyl ether. The resulting white slurry was stirred and allowed to warm gradually to room temperature overnight. The reaction was then quenched with an argon-saturated aqueous solution of NH_4Cl (33 mL of a 54.4 g L^{-1} solution). Upon stirring, all precipitate dissolved. The organic phase was cannulated into a flask containing $MgSO_4$, along with two pentane washings (30 mL each) of the aqueous layer. After drying over $MgSO_4$ for 1 h, the product was filtered into a round-bottomed flask equipped with a magnetic stirrer, along with two pentane washings (50 mL each) of the $MgSO_4$. The organic solvents were distilled off at room pressure to yield a colourless liquid (64.6 g, 0.403 mol, 96%). ^{1}H NMR (500 MHz, $CDCl_3$, 298 K): δ 1.02 (d, $^3J_{PH} = 11$ Hz, 18H, ^{t}Bu), 0.87 (d, $^2J_{PH} = 4$ Hz, 3H, Me). ^{31}P{^{1}H} NMR (202.5 MHz, $CDCl_3$, 298 K): δ 12.2 (s).

Step 4: $(^tBu)_2PCH_2Li.^{51}$. *tert*-Butyl lithium (280 mL of a 1.7 M solution in pentane, 0.476 mol) was transferred to a 500 mL round-bottomed flask with a blown-glass frit equipped with a magnetic stirrer, and the solvent was removed under vacuum. The $(^tBu)_2PMe$ from the previous step (56.0 g, 0.348 mol) was dissolved in heptane (200 mL) and added. The mixture was heated to reflux for a total of 18 h, resulting in an orange solution and pale yellow precipitate. A further 200 mL of heptane was added and the slurry was filtered through the attached frit at room temperature, then washed with pentane (3 × 300 mL) and dried under vacuum. Total yield of pale tan solid: 52.2 g, 0.314 mol (90%). ^{31}P{^{1}H} NMR (121.5 MHz, THF-d_8, 298 K): δ 45.2 (s).

Step 5: $(^tBu)_2PCH_2P(^tBu)_2$. The solid lithium methanide from the previous step (52.2 g, 0.314 mol) was weighed into a round-bottomed flask equipped with a magnetic stirrer bar in an argon-filled dry box and suspended in THF (1 L). After cooling the flask to −78 °C, $^tBu_2PCl$ (52.1 mL, 56.4 g, 0.313 mol) was added and the mixture was stirred and allowed to warm gradually to room temperature overnight. The THF was distilled off at room pressure, and the product was extracted into pentane (100 mL). Hydrolysis with NH_4Cl (80 mL of a 4% solution in argon-saturated water) caused the solution to warm. The organic phase, including two 100 mL pentane washings of the aqueous phase, was dried over $MgSO_4$ and filtered, and the pentane was distilled off at room pressure resulting in a yellow oil. Dissolution in methanol and cooling to −10 °C led to the crystallisation of the product as colourless needles. Yield: 74.0 g (0.243 mol, 77%). Anal. calcd for $C_{17}H_{38}P_2$: C, 67.07; H, 12.58; P, 20.35; found: C, 67.11; H, 12.66; P, 20.33. Mp: 45–46 °C. Bp: 75–80 °C/10^{-3} mm. ^{1}H NMR (300 MHz, C_6D_6, 298 K): δ 1.61 (t, $^2J_{PH} = 1.8$ Hz, 2H, CH_2), 1.19 ("t", $^{3+5}J_{PH} = 10.3$ Hz, 36H, ^{t}Bu). ^{31}P{^{1}H} NMR (121.5 MHz, C_6D_6, 298 K): δ 21.3 (s). ^{13}C{^{1}H} NMR (75.7 MHz, C_6D_6, 298 K): δ 32.6 (dd, $^1J_{PC} = 10.8$ Hz, $^3J_{PC} = 9.8$ Hz, CMe_3), 30.1 ("t", $^{2+4}J_{PC} = 15.7$ Hz, CH_3), 12.7 (t, $^1J_{PC} = 36.2$ Hz, CH_2). IR (KBr pellet, cm^{-1}): 2900 (br, vs), 1459 (br, vs), 1385 (s), 1362 (vs), 1174 (br, vs), 1130 (m), 1017 (s), 982 (w), 930 (m), 808 (vs), 785 (s), 714 (s), 672 (s), 588 (m), 461 (m), 425 (m).

2. This ligand can be prepared in an analogous manner to **1** *via* Cy_2PCH_2Li, with a yield in the final step of 83%. Two other routes are published.[38,40] Mp: 95–97 °C. Anal. calcd for $C_{25}H_{46}P_2$: C, 73.49; H, 11.35; P, 15.16; found: C, 73.10; H, 11.34; P, 15.00.

3. Dicyclohexylchlorophosphine was used in step 3 and the product was isolated in 53% yield as white crystals from pentane. Mp: 46–47 °C. Anal. calcd for $C_{21}H_{42}P_2$: C, 70.75; H, 11.87; found: C, 70.52; H, 11.88. ^{31}P{^{1}H} NMR (202.5 MHz, CD_2Cl_2, 300 K): δ 18.9 [d, $^2J_{PP} = 108$ Hz, P(^{t}Bu)$_2$], −5.7 (d, $^2J_{PP} = 108$ Hz, PCy_2). Further characterisation

details are not included as an alternative synthesis has been published.[38]

4. Di(*iso*-propyl)chlorophosphine was used in step 3 and the product was isolated as a colourless liquid in 92% yield. ^{31}P NMR (122 MHz, $CDCl_3$, 298 K): δ 19.31 [d, $^2J_{PP} = 98$ Hz, P(^{t}Bu)$_2$], 3.03 [d, $^2J_{PP} = 98$ Hz, P(^{i}Pr$_2$)]. MS (CI+): $m/z = 277$ (M + H)$^+$ with the correct isotope pattern. Further characterisation details are not included as an alternative synthesis has been published.[38]

5. Diphenylchlorophosphine was used in step 3 and the product was isolated from pentane in 88% yield as white crystals, which melt at 40 °C. Two other routes are also published.[36,37] Anal. calcd for $C_{21}H_{30}P_2$: C, 73.2; H, 8.78; P, 18.0; found: C, 73.4; H, 8.87; P, 17.7. ^{1}H NMR (300 MHz, $CDCl_3$, 298 K): δ 7.54 (m, 4H, *m*-C_6H_5), 7.36 (m, 6H, *o/p*-C_6H_5), 2.12 (s, 2H, CH_2), 1.14 (d, $^3J_{PH} = 10.9$ Hz, 18H, ^{t}Bu). ^{31}P{^{1}H} NMR (122 MHz, CD_2Cl_2, 298 K): δ 15.9 [d, $^2J_{PP} = 139.5$ Hz, P(^{t}Bu)$_2$], −16.0 (d, $^2J_{PP} = 139.5$ Hz, PPh_2). ^{13}C{^{1}H} NMR (75 MHz, CD_2Cl_2, 298 K): δ 140.3 (dd, $^1J_{PC} = 16.6$ Hz, $^3J_{PC} = 7.6$ Hz, C_{ipso}), 133.4 (d, $^2J_{PC} = 19.4$ Hz, C_o), 128.8 (s, C_p), 128.5 (d, $^3J_{PC} = 6.9$ Hz, C_m), 32.0 [dd, $^1J_{PC} = 24.2$ Hz, $^3J_{PC} = 6.9$ Hz, $C(CH_3)_3$], 29.8 ([dd, $^2J_{PC} = 13.8$ Hz, $^4J_{PC} = 2.1$ Hz, $C(CH_3)_3$], 20.6 (dd, $^1J_{PC} = 20.8$ Hz, $^1J_{PC} = 33.9$ Hz, CH_2). IR (KBr, cm^{-1}): 3069 w, 3055 w, 2947 s, 2893 m, 2860 m, 1585 w, 1465 m, 1433 s, 1387 w, 1365 m, 1176 m, 1093 w, 1067 w, 999 w, 809 m, 767 w, 736 s, 695 s, 507 m, 476 m. MS (CI+): $m/z = 345$ (M + H)$^+$ with the correct isotope pattern.

7. The diphosphine **1** (2.0 g, 6.6 mmol) was dissolved in pentane (20 mL) in a Schlenk tube equipped with a reflux condenser and a magnetic stirrer bar. At reflux, 15 mL of a 30% hydrogen peroxide solution was added. After stirring for 2 h at reflux and cooling to room temperature, the pentane phase was removed *via* cannula and the aqueous phase was washed with pentane (2 × 2 mL). The combined organic phases were dried over $MgSO_4$, filtered and concentrated under reduced pressure. The oily product was then distilled under vacuum at 230–240 °C and the distillate was crystallised from a pentane–diethyl ether mixture at 0 °C. Yield: 1.9 g, 85%. Mp: 122 °C. Anal. calcd for $C_{17}H_{38}P_2O_2$: C, 60.67; H, 11.39; found: C, 60.39; H, 11.42. ^{1}H NMR (300 MHz, $CDCl_3$, 298 K): δ 2.10 (t, $^2J_{PH} = 12.8$ Hz, 2H, CH_2), 1.31 (d, $^3J_{PH} = 14.0$ Hz, 36H, ^{t}Bu). ^{31}P{^{1}H} NMR (121.5 MHz, CD_2Cl_2, 298 K): δ 59.7 (s). ^{13}C{^{1}H} NMR (75 MHz, CD_2Cl_2, 298 K): δ 36.7 [dd, $^1J_{PC} = 34$ Hz, $^3J_{PC} = 6.2$ Hz, $PC(CH_3)_3$], 26.9 [s, $C(CH_3)_3$], 16.1 ("t", $^1J_{PC} = 40.5$ Hz, CH_2). IR (KBr, cm^{-1}): 2954 (vs, CH), 2903 (vs, CH), 2871 (vs, CH), 1158 (vs, PO). MS (CI+): $m/z = 337.2$ (M)$^+$ with the correct isotope pattern.

$[8^+][B(3,5\text{-}(CF_3)_2C_6H_3)_4]^-$. In a glove box, $[H(OEt_2)_2][BAr_F]$ (108 mg, 0.107 mmol) and **1** (37 mg, 0.122 mmol) were weighed together into a 20 mL Schlenk flask equipped with a magnetic stirrer bar. Diethyl ether (2 mL) was added and the resulting clear, colourless solution was stirred at room temperature for 10 min. Addition of hexane (2 mL) resulted in the precipitation of a white solid, which was isolated and washed twice with hexane. The fine white powder was dried under dynamic vacuum. The compound can be recrystallised from ether–hexane (1:1) at −20 °C. Yield: 98 mg, 70%. Mp: 110–111 °C (decomposition). ^{1}H NMR (300 MHz, THF-d_8, 298 K): δ 7.82 (s, 8H, *o*-BAr_F), 7.60 (s, 4H, *p*-BAr_F), 5.97 (dt, $^1J_{H,P} = 461.5$ Hz, $^3J_{H,H} = 6.4$ Hz, 1H, HPR_3), 2.27 (ddd, $^3J_{H,H} = 6.4$ Hz, $^2J_{P,H} = 14.5$ Hz, $^2J_{P,H} = 2.0$ Hz, 2H, $^tBu_2HPCH_2P^tBu_2$), 1.63 (d, $^2J_{P,H} = 16.5$ Hz, 9H, $^tBu_2HPCH_2P^tBu_2$), 1.29 (d, $^2J_{P,H} = 16.5$ Hz, 9H, $^tBu_2HPCH_2P^tBu_2$). ^{31}P{^{1}H} NMR (THF-d_8, 121.5 MHz, 298 K): δ 26.6 (d, $^2J_{P,P} = 40.0$ Hz, $^tBu_2HPCH_2P^tBu_2$), 47.6 (d, $^2J_{P,P} = 40.0$ Hz, $^tBu_2HPCH_2P^tBu_2$). ^{13}C{^{1}H} NMR

(THF-d_8, 75.5 MHz, 298 K): δ 162.8 (q, J_{BC} = 50.1 Hz, *i*-C BAr$_F$), 135.9 (br, *o*-C BAr$_F$), 129.6 (q, $^3J_{C,F}$ = 49 Hz, *m*-C BAr$_F$), 124.6 (q, $^1J_{C,F}$ = 272 Hz, CF$_3$), 118.5 (s, *p*-C BAr$_F$), 35.7 [m, P*C*(CH$_3$)$_3$], 34.5 [m, P*C*(CH$_3$)$_6_3$], 30.0 [d, $^2J_{PC}$ = 14.5 Hz, PC(*C*H$_3$)$_3$], 28.4 [d, $^2J_{PC}$ = 4.15 Hz, PC(*C*H$_3$)$_3$], 7.1 (dd, $^1J_{PC}$ = 41.5 Hz, $^1J_{PC}$ = 53.6 Hz, HP*C*H$_2$P).

[9$^+$][Fe$_2$Cl$_6$]$_{1/2}$$^-$. This salt was isolated as a by-product in an attempt to prepare (dtbpm-κ^2P)FeCl$_2$; no attempts were made to optimise the synthesis of **9$^+$**. (CO)$_4$FeCl$_2$ (180 mg, 0.754 mmol) was suspended in toluene (10 mL) at $-25\,^\circ$C. A solution of **1** (250 mg, 0.821 mmol, 1.1 equiv.) was added *via* cannula. Gas evolution was immediately observed and the colour changed from yellow to red and then to green. After addition of **1** was complete the solution was stirred for 30 min at $-25\,^\circ$C, then allowed to warm to room temperature and stirred for a further 3 h. During this time, a yellow precipitate was observed. The mother liquor was removed *via* cannula and cooled to $-25\,^\circ$C, which led to the crystallisation of yellow (dtbpm-κ^2P)Fe(CO)$_3$. The residual yellow precipitate was dissolved in CH$_2$Cl$_2$ and cooling led to the formation of a small quantity of pale yellow X-ray quality crystals of [^{t}Bu$_2$P(Cl)CH$_2$P^{t}Bu$_2$]$^+$[Fe$_2$Cl$_6$]$_{1/2}$$^-$·CH$_2Cl_2$. No further characterisation was conducted.

Crystallographic studies

For each compound studied by X-ray diffraction, crystals were grown by slow cooling of a concentrated pentane or methanol solution of the compound. A crystal was mounted on a glass fibre with perfluoropolyether. All measurements other than for dcpm (**2**) were made on a Siemens SMART diffractometer with graphite monochromated Mo-Kα radiation using a CCD detector. Frames corresponding to a sphere of data were collected using the ω-scan technique; in each case, 20 s exposures of 0.3° in ω were taken. The reflections were integrated using SAINT.[82] An absorption correction was applied to each structure other than **1** (for reasons described below) using SADABS[83] and the data were corrected for Lorentz and polarisation effects. The space groups were determined by the systematic absences of *hkl* values using XPREP (Siemens, SHELXTL 5.04). The structures were solved by direct methods and expanded using Fourier techniques. All non-hydrogen atoms were refined anisotropically; hydrogen atoms were included in calculated positions and not refined except for in the structure of **2**. The final cycle of full-matrix least-squares refinement converged. The function minimised was $\Sigma w[(F_o)^2 - (F_c)^2]^2$. All calculations were performed using the SHELXTL crystallographic software package of Bruker.[84]

CCDC reference numbers 199933–40. See http://www.rsc.org/suppdata/nj/b2/b210114a/ for crystallographic files in CIF or other electronic format.

dtbpm (1). The skeleton of the molecule is disordered over two orientations with almost the same occupancy, and the bulky *tert*-butyl groups are located in roughly the same space in the unit cell for both orientations. This disorder leads to a pseudo-mirror plane. Therefore, the structure could be modelled either in the centrosymmetric space group P*nma* (#62) with the mirror plane, or in the less-symmetric space group P*na*2$_1$ (#33). The latter was chosen, as use of the higher symmetry space group led to problems with special positions. The disorder was modelled as two independent molecular geometries, constrained to have the same bond lengths and angles, which refined with occupancies of 54 and 46%. The structural details described above correspond to the higher-occupancy orientation. However, the disorder means that the accuracy of the solution is low, and no absorption correction was applied.

dcpm (2). The structure was measured on an Enraf–Nonius CAD-4 diffractometer. The space group P$\bar{1}$ (#2) was confirmed by successful solution and refinement of the structure. No absorption correction was applied. Hydrogen atoms were refined isotropically.

dtbpe (6). The asymmetric unit consists of half the molecule, with the middle of the ethylene bridge lying on an inversion centre.

^{t}Bu$_2$P(O)CH$_2$P(O)^{t}Bu$_2$ (7). Two independent, geometrically similar molecules form the asymmetric unit.

[^{t}Bu$_2$P(H)CH$_2$P^{t}Bu$_2$]$^+$[B(3,5-(CF$_3$)$_2$C$_6$H$_3$)$_4$]$^-$ (the cation of which is 8$^+$). The hydrogen atom on P1 was clearly seen in the difference map and allowed to refine freely. Some disorder of the CF$_3$ groups of the anion was observed, as is characteristic with this anion.

[^{t}Bu$_2$P(Cl)CH$_2$P^{t}Bu$_2$]$^+$[Fe$_2$Cl$_6$]$_{1/2}$$^-$·CH$_2Cl_2$ (the cation of which is 9$^+$). The counter ion lies on a special position and is present in the crystal as one [Fe$_2$Cl$_6$]$^{2-}$ with two bridging chlorides per two phosphine cations.

Computational methods

Complete geometry optimisations for **1**–**9$^+$** were carried out using 2.5 GHz Dell PCs at the restricted Hartree–Fock level using program systems Gaussian 98 as implemented in Gaussian 98W,[85] and Jaguar (Jaguar 3.5, Schrödinger, Inc. Portland, Oregon, 2001) as implemented in Titan 1.05 (Wavefunction, Inc., Schrödinger, Inc, 2001). Minimum structures have been verified by vibrational frequency calculations (NIMAG = 0).

Acknowledgements

References

1 As in earler work, we use the shorthand notation dtbpm for bis(di-*tert*-butylphosphino)methane (**1**) and analogously derived acronyms for the other systems.

2 P. Dierkes and P. W. N. M. van Leeuwen, *J. Chem. Soc., Dalton Trans.*, 1999, 1519–1529.

3 R. M. Beesley, C. K. Ingold and J. F. Thorpe, *J. Chem. Soc.*, 1915, **107**, 1080–1106.

4 B. Chaudret, B. Delavaux and R. Poilblanc, *Coord. Chem. Rev.*, 1988, **86**, 191–243.

5 J. T. Mague, *J. Cluster Sci.*, 1995, **6**, 217–269.

6 G. M. Ferrence, P. E. Fanwick, C. P. Kubiak and R. J. Haines, *Polyhedron*, 1997, **16**, 1453–1459.

7 B. F. Straub, F. Rominger and P. Hofmann, *Inorg. Chem.*, 2000, **39**, 2113–2119.

8 S. M. Reid, J. T. Mague and M. J. Fink, *J. Am. Chem. Soc.*, 2001, **123**, 4081–4082.

9 P. Hofmann, C. Meier, U. Englert and M. U. Schmidt, *Chem. Ber.*, 1992, **125**, 353–365.

10 T. Nickel, R. Goddard, C. Krüger and K.-R. Pörschke, *Angew. Chem., Int. Ed. Engl.*, 1994, **33**, 879–882.

11 B. F. Straub, F. Rominger and P. Hofmann, *Inorg. Chem. Commun.*, 2000, **3**, 358–360.

12 N. Simhai, C. N. Iverson, B. L. Edelbach and W. D. Jones, *Organometallics*, 2001, **20**, 2759–2766.

13 P. Hofmann, H. Heiss, P. Neiteler, G. Müller and J. Lachmann, *Angew. Chem., Int. Ed. Engl.*, 1990, **29**, 880–882.
14 P. Hofmann and G. Unfried, *Chem. Ber.*, 1992, **125**, 659–661.
15 G. Scherhag, Dissertation, Ruprecht-Karls Universität Heidelberg, Heidelberg, 2001.
16 P. Hofmann, H. Heiss and G. Müller, *Z. Naturforsch., B: Chem. Sci.*, 1987, **42**, 395–409.
17 P. Hofmann, L. A. Perez-Moya, M. E. Krause, O. Kumberger and G. Müller, *Z. Naturforsch., B: Chem. Sci.*, 1990, **45**, 897–908.
18 P. Hofmann, L. A. Perez-Moya, O. Steigelmann and J. Riede, *Organometallics*, 1992, **11**, 1167–1176.
19 B. F. Straub and P. Hofmann, *Inorg. Chem. Commun.*, 1998, **1**, 350–353.
20 B. F. Straub, F. Rominger and P. Hofmann, *Inorg. Chem. Commun.*, 2000, **3**, 214–217.
21 S. M. Hansen, M. A. O. Volland, F. Rominger, F. Eisenträger and P. Hofmann, *Angew. Chem., Int. Ed.*, 1999, **38**, 1273–1276.
22 M. A. O. Volland, C. Adlhart, C. A. Kiener, P. Chen and P. Hofmann, *Chem.-Eur. J.*, 2001, **7**, 4621–4632.
23 D. B. Grotjahn, G. A. Bikzhanova, L. S. B. Collins, T. Concolino, K.-C. Lam and A. L. Rheingold, *J. Am. Chem. Soc.*, 2000, **122**, 5222–5223.
24 H. Urtel, G. A. Bikzhanova, D. B. Grotjahn and P. Hofmann, *Organometallics*, 2001, **20**, 3938–3949.
25 H. Urtel, C. Meier, F. Eisenträger, F. Rominger, J. Joschek and P. Hofmann, *Angew. Chem., Int. Ed.*, 2001, **40**, 781–784.
26 F. Lippert and A. Höhn and P. Hofmann, *World Pat.* WO 96/37537, 1996 (BASF AG).
27 F. Lippert, A. Höhn and P. Hofmann, *World Pat.* WO 96/37536, 1996 (BASF AG).
28 F. Lippert, A. Höhn and P. Hofmann, *World Pat.* WO 95/03353, 1995 (BASF AG).
29 F. Lippert, A. Höhn and E. Schauss, *World Pat.* WO 96/37522, 1996 (BASF AG).
30 N. A. Cooley, S. M. Green, D. F. Wass, K. Heslop, A. G. Orpen and P. G. Pringle, *Organometallics*, 2001, **20**, 4769–4771.
31 M. Schultz, F. Eisenträger, C. Regius, F. Rominger and P. Hofmann, in preparation.
32 I. D. Gridnev, Y. Yamanoi, N. Higashi, H. Tsuruta, M. Yasutake and T. Imamoto, *Adv. Synth. Catal.*, 2001, **343**, 118–136.
33 H. H. Karsch, *Z. Naturforsch., B: Anorg. Chem. Org. Chem.*, 1983, **38**, 1027–1030.
34 P. Hofmann and H. Heiss, *Ger. Pat.* DE 41 34 772, 1991 (BASF AG).
35 J. Feldman, E. Hauptman, E. F. McCord and M. S. Brookhart, *World Pat.* WO 98/47934, 1998 (Du Pont).
36 S. O. Grim, P. H. Smith, I. J. Colquhoun and W. McFarlane, *Inorg. Chem.*, 1980, **19**, 3195–3198.
37 L. Weber and D. Wewers, *Chem. Ber.*, 1984, **117**, 1103–1112.
38 J. Wolf, M. Manger, U. Schmidt, G. Fries, D. Barth, B. Weberndörfer, D. A. Vicic, W. D. Jones and H. Werner, *J. Chem. Soc., Dalton Trans.*, 1999, 1867–1875.
39 K. Jonas, preparation of dcpm, personal communication, 1988.
40 F. L. Joslin, J. T. Mague and D. M. Roundhill, *Polyhedron*, 1991, **10**, 1713–1715.
41 I. P. Rothwell, the hydrogenation requires well over one equivalent of catalyst (personal communication), 2000.
42 J. S. Yu and I. P. Rothwell, *J. Chem. Soc., Chem. Commun.*, 1992, 632–633.
43 M. F. Lappert, J. B. Pedley, B. T. Wilkins, O. Stelzer and E. Unger, *J. Chem. Soc., Dalton Trans.*, 1975, 1207–1214.
44 B. L. Shaw, *J. Chem. Soc., Chem. Commun.*, 1979, 104–105.
45 G. M. Bancroft, L. Dignard-Bailey and R. J. Puddephatt, *Inorg. Chem.*, 1986, **25**, 3675–3680.
46 D. L. Lichtenberger and M. E. Jatcko, *Inorg. Chem.*, 1992, **31**, 451–455.
47 M. J. S. Dewar, E. G. Zoebisch, F. Eamonn and J. J. P. Stewart, *J. Am. Chem. Soc.*, 1985, **107**, 3902–3909.
48 K. Issleib and W. Seidel, *Chem. Ber.*, 1959, **92**, 2681–2694.
49 M. Fild, O. Stelzer and R. Schmutzler, *Inorg. Synth.*, 1973, **14**, 4–9.
50 H. Gilman and F. K. Cartledge, *J. Organomet. Chem.*, 1964, **2**, 447–454.
51 H. H. Karsch and H. Schmidbaur, *Z. Naturforsch., B: Anorg. Chem. Org. Chem.*, 1977, **32**, 762–767.
52 A large centrifuge, which can be used with the exclusion of air from the flask, could also be used if available.
53 P. Hofmann, C. Meier, W. Hiller, M. Heckel, J. Riede and M. U. Schmidt, *J. Organomet. Chem.*, 1995, **490**, 51–70.
54 Solid-state structures containing a κ^2-dtbpm chelate ligand bound to Ni, Pd, Pt, Fe, Ru, Rh and Ir have been determined in our group.
55 K. Issleib and D.-W. Müller, *Chem. Ber.*, 1959, **92**, 3175–3182.
56 W. Hewertson and H. R. Watson, *J. Chem. Soc.*, 1962, 1490–1494.
57 H. Schmidbaur, G. Reber, A. Schier, F. E. Wagner and G. Müller, *Inorg. Chim. Acta*, 1988, **147**, 143–150.
58 J. Bruckmann and C. Krüger, *Acta Crystallogr., Sect. C*, 1995, **51**, 1155–1158.
59 J. Bruckmann and C. Krüger, *Acta Crystallogr., Sect. C*, 1995, **51**, 1152–1155.
60 F. M. Conroy-Lewis, L. Mole, A. D. Redhouse, S. A. Litster and J. L. Spencer, *J. Chem. Soc., Chem. Commun.*, 1991, 1601–1603.
61 I. Bach, K.-R. Pörschke, R. Goddard, C. Kopiske, C. Krüger, A. Rufinska and K. Seevogel, *Organometallics*, 1996, **15**, 4959–4966.
62 I. Bach, K.-R. Pörschke, B. Proft, R. Goddard, C. Kopiske, C. Krüger, A. Rufinska and K. Seevogel, *J. Am. Chem. Soc.*, 1997, **119**, 3773–3781.
63 I. Bach, R. Goddard, C. Kopiske, K. Seevogel and K.-R. Pörschke, *Organometallics*, 1999, **18**, 10–20.
64 D. J. Mindiola and G. L. Hillhouse, *J. Am. Chem. Soc.*, 2001, **123**, 4623–4624.
65 D. Mindiola and G. Hillhouse, *J. Am. Chem. Soc.*, 2002, **124**, 9976–9977.
66 R. Melenkivitz, D. Mindiola and G. Hillhouse, *J. Am. Chem. Soc.*, 2002, **124**, 3846–3847.
67 R. Trebbe, R. Goddard, A. Rufinska, K. Seevogel and K.-R. Pörschke, *Organometallics*, 1999, **18**, 2466–2472.
68 N. Carr, B. J. Dunne, L. Mole, A. G. Orpen and J. L. Spencer, *J. Chem. Soc., Dalton Trans.*, 1991, 863–871.
69 T. Gottschalk-Gaudig, J. C. Huffman and K. G. Caulton, *J. Am. Chem. Soc.*, 1999, **121**, 3242–3243.
70 T. Gottschalk-Gaudig, J. C. Huffman, H. Gérard, O. Eisenstein and K. G. Caulton, *Inorg. Chem.*, 2000, **39**, 3957–3962.
71 M. A. O. Volland, B. F. Straub, I. Gruber, F. Rominger and P. Hofmann, *J. Organomet. Chem.*, 2001, **617–618**, 288–291.
72 D. W. H. Rankin, H. E. Robertson, R. Seip, H. Schmidbaur and G. Blaschke, *J. Chem. Soc., Dalton Trans.*, 1985, 827–830.
73 H. A. Bent, *J. Chem. Educ.*, 1960, **37**, 616–624.
74 H. A. Bent, *Chem. Rev.*, 1961, **61**, 275–311.
75 M. A. O. Volland, Dissertation, Ruprecht-Karls Universität Heidelberg, Heidelberg, 2001.
76 T. P. Debies and J. W. Rabalais, *Inorg. Chem.*, 1974, **13**, 308–312.
77 S. Ikuta, P. Kebarle, G. M. Bancroft, T. Chan and R. J. Puddephatt, *J. Am. Chem. Soc.*, 1982, **104**, 5899–5902.
78 D. E. Cabelli, A. H. Cowley and M. J. S. Dewar, *J. Am. Chem. Soc.*, 1981, **103**, 3286–3289.
79 R. Hoffmann, *Acc. Chem. Res.*, 1971, **4**, 1–9.
80 K.-R. Pörschke, C. Pluta, B. Proft, F. Lutz and C. Krüger, *Z. Naturforsch., B: Chem. Sci.*, 1993, **48**, 608–626.
81 W. Hieber and G. Bader, *Chem. Ber.*, 1928, **61**, 1717–1722.
82 SAINT, v. 4.024: Siemens Industrial Automation, Inc, Madison, WI, 1995.
83 G. M. Sheldrick, SADABS, Bruker AXS, Inc., Madison, WI, 1996.
84 G. M. Sheldrick, SHELXTL Crystal Structure Determination Package, Bruker AXS, Inc, Madison, WI, 1997.
85 M. J. Frisch, G. W. Trucks, H. B. Schlegel, G. E. Scuseria, M. A. Robb, J. R. Cheeseman, V. G. Zakrzewski, J. A. Montgomery, R. E. Stratmann, J. C. Burant, S. Dapprich, J. M. Millam, A. D. Daniels, K. N. Kudin, M. C. Strain, O. Farkas, J. Tomasi, V. Barone, M. Cossi, R. Cammi, B. Mennucci, C. Pomelli, C. Adamo, S. Clifford, J. Ochterski, G. A. Petersson, P. Y. Ayala, Q. Cui, K. Morokuma, D. K. Malick, A. D. Rabuck, K. Raghavachari, J. B. Foresman, J. Cioslowski, J. V. Ortiz, A. G. Baboul, B. B. Stefanov, G. Liu, A. Liashenko, P. Piskorz, I. Komaromi, R. Gomperts, R. L. Martin, D. J. Fox, T. Keith, M. A. Al-Laham, C. Y. Peng, A. Nanayakkara, C. Gonzalez, M. Challacombe, P. M. W. Gill, B. Johnson, W. Chen, M. W. Wong, J. L. Andres, C. Gonzalez, M. Head-Gordon, E. S. Replogle and J. A. Pople, Gaussian 98, revision A.9, Gaussian, Inc., Pittsburgh, PA, 1998.